RSC Advances

PAPER

View Article Online
View Journal | View Issue

Cite this: *RSC Adv.*, 2021, **11**, 37375

Naproxen release aspect from boron-doped carbon nanodots as a bifunctional agent in cancer therapy†

Aswandi Wibrianto,[a] Dinar F. Putri,[a] Satya C. W. Sakti,[ab] Hwei V. Lee[c] and Mochamad Z. Fahmi*[ab]

Received 14th August 2021
Accepted 1st November 2021

DOI: 10.1039/d1ra06148h

rsc.li/rsc-advances

In this present study, boron–carbon nanodots were synthesized by the hydrothermal method. Boron–carbon nanodots were prepared by varying the concentration ratios of boronic acid and citric acid: 1 : 25, 2 : 1, and 25 : 1, respectively. The precursors were then poured into a Teflon autoclave and heated at 240° for 4 h. This research aims to synthesise and evaluate the potential of boron–carbon nanodots as a bioimaging agent and naproxen delivery carrier. An X-ray diffractogram showed that the boron–carbon nanodots were amorphous. To analyse the functional groups, FTIR and XPS analysis was carried out. Spectrofluorometric analysis (λ_{ex} 320 nm) showed that the formulation of boron–carbon nanodots 2 : 1 (BCD 2 : 1) has the most ideal fluorescent properties at λ_{em} 453 nm, whereas UV-vis analysis showed λ_{max} at 223 nm, with a quantum yield of 52.29%. A confocal laser scanning micrograph and toxicity test (MTT assays) showed that boron–carbon nanodots delivered naproxen efficiently with loading amount and loading efficiency of naproxen 28% and 65%, respectively. Furthermore, it induced an anticancer effect in HeLa cells. This result indicated that boron–carbon nanodots can be used as a bioimaging agent and naproxen delivery carrier.

Introduction

Nanoparticle carbon nanodots (CDS) are nanoparticles that are in high demand and are developing very rapidly. According to previous research,[1] CDS has high solubility, is non-toxic, and has bright luminescence, so it can be used for various applications, including bio-imaging, sensors, drug delivery, catalysts, and photovoltaic devices.[2] CDS can be synthesized from carbon materials such as carbohydrates, proteins, amino acids,[3] and biopolymers with chemical ablation, electrochemical,[4] laser ablation, microwave radiation, hydrothermal,[5] solvothermal,[6] and pyrolysis methods.[7] Synthesized CDS are possible to utilize directly in various fields without any modifications, such as in the fields of biomedicine,[8] photonics, catalysts, and sensors.[9,10] However, the photo-optical properties of this material do not perform very well. To enhance the optical properties of CDS, the surface modification precursors should be combined with other materials to generate better outcomes.

Doped-CDS can be a versatile material for future biomedical and bioimaging applications with unique fluorescence properties,[11] excellent biocompatibility, and high water solubility.[12] Besides acting as a bioimaging agent, CDS can function as a drug delivery carrier, a substance used in the process of delivering chemical compounds or drugs to achieve targets or therapeutic effects in humans.[13] The fabrication procedure of doped-CDS is quite simple and low-cost due to the wide choice of cheap carbon sources.

Heteroatom materials commonly used in doping CDS are boron (B), nitrogen (N), sulphur (S), and phosphorus (P) atoms. Boron atoms are neighbouring elements of atom carbon in the periodic table that have atomic radii and similar atomic structures.[14] Moreover, boron doping on CDS progressively increasing the quantum yield of CDS owing to the p-type semiconductor effect, which comes from the boron elements. According to previous research, boron–carbon nanodots are not widely used in the field of bioimaging, but rather are applied in the detection of metal ions by the colorimetric method,[15] detections of *p*-nitrophenol,[16] dopamine examination,[17] and sensors for acetone and dopamine.[18] Therefore, this research will report the results of synthesis and characterization of CDS nanoparticles doped with boron atoms using the hydrothermal method as a candidate for bioimaging agents and naproxen delivery systems in HeLa cancer cells.

Experimental

Materials

Citric acid ($C_6H_8O_7$; 99.5%; Merck), boric acid (H_3BO_3; 99.5%; Sigma Aldrich), sodium hydroxide (NaOH; Sigma Aldrich), naproxen sodium ($C_{14}H_{13}NaO_3$; Sigma Aldrich), Dulbecco's Modified Eagle Medium (DMEM, 98%; Sigma Aldrich), phosphate buffered

[a]*Department of Chemistry, Universitas Airlangga, Surabaya 61115, Indonesia. E-mail: m.zakki.fahmi@fst.unair.ac.id; Fax: +62-31-5922427; Tel: +62-31-5922427*

[b]*Supramodification Nano-Micro Engineering Research Group, Universitas Airlangga, Surabaya 60115, Indonesia*

[c]*Nanotechnology and Catalysis Research Centre, Institute of Postgraduate Studies (IPS), University of Malaya, Kuala Lumpur, 50603, Malaysia*

† Electronic supplementary information (ESI) available: Solid phase of synthesized BCD; the size distribution histogram; TEM images; turbidity data the cytotoxicity concentration of BCD; all theoretical and experimental plot of naproxen release. See DOI: 10.1039/d1ra06148h

saline (PBS; 99%; Sigma Aldrich), demineralized water and 3- salts [4,5-dimethylthiazol-2-yl]-2,5-diphenyl tetrazolium bromide (MTT). All chemicals were used directly without further purification.

Synthesis of doping CDS

The synthesis of boron–carbon nanodots (BCD) begins with mixing citric acid and boric acid with variations in the concentration ratio of boric acid are citric acid, which is 25 : 1, 2 : 1, and 1 : 25, respectively. The variation for CDS fabrication was referred to previous research.[19] Citric acid weighed 0.0899 grams each; 0.2667 grams and 0.0101 grams. While boric acid weighed 0.0101 grams each; 0.1500 grams and 0.0899 grams. After that, citric acid and boric acid are put into a glass vial and 2 mL of water is added. This process produces a colourless solution. Then, the vial is inserted into a device called a Teflon autoclave. Next, the Teflon autoclave was put into the Daihan Scientific furnace for 4 h at 240 °C. Besides that, BCDS were synthesized using the same method without the addition of boric acid as a comparison. The products were then dissolved with NaOH 0.1 N after the cooling process at room temperature. The solution then was further dialyzed on the membrane with a molecular weight cut-off (MWCO) of 1 kDa to specify the CDs size distribution and exclude by-products.[14]

Synthesis of naproxen-loaded BCDS (N-BCD)

The synthesis of naproxen-loaded BCDS starts with mixing boron–carbon nanodots as much as 0.2 grams into 25 mL NaOH. Then 0.02 grams of naproxen were mixed to the solution and stirred for 24 h. Unconnected naproxen further removed from the colloidal mixture (N-BCD) by dialysis membrane MWCO 1000 Da. Further the percentage of loading efficiency (LE) and loading amount (LA) are determined through following equations:

$$\text{LE } (\%) = \frac{\text{mass of Dox on FA} - \text{CD}}{\text{mass of Dox in feed}} \times 100\% \quad (1)$$

$$\text{LA } (\%) = \frac{\text{mass of Dox on FA} - \text{CD}}{\text{mass of FA} - \text{CD}} \times 100\% \quad (2)$$

Cytotoxicity evaluation

The cytotoxicity data BCD and naproxen-loaded BCD was acquired through MTT assay in HeLa cancer cells. HeLa cells previously cultured in Eagle's minimum essential medium were placed in a 96-well plate and incubated for 24 h at 37 °C under 5% CO_2. The proliferated cells were washed with phosphate-buffered saline (PBS, Biogear Scientific, Netherland) and incubated with samples for 24 h. It was followed by adding the MTT reagent (1 mL, 500 mg mL^{-1}) and incubated for 4 h. The absorbance of the formed formazan crystals was measured at 570 nm after being dissolved in dimethyl sulfoxide using an ELISA reader (Azure Biosystem). The absorbance intensity was related to the number of living cells, and cell viability data was collected.

Confocal imaging observation

HeLa cells were incubated with boron–carbon nanodots (400 μL) samples for 60 min after being placed in 96-well plates with Dulbecco's Modified Eagle Medium (DMEM) media and incubated for 24 h. The treated cells are then washed with a solution of phosphate buffered saline (PBS) and fixed with 70% alcohol for 10 minutes. Fluorescence images were obtained from cells for immersion of 63 × 1.32 NA oil using TCS SP2 confocal (Leica Microsystems, USA) equipped with an inverted microscope and inline Ar (488 nm) and He–Ne (503–680 nm and 588 nm) laser.

Kinetic release assessment

To verify the kinetic release of naproxen, boron–carbon nanodots (3 mL) samples were placed in MWCO (40 kDa) dialysis membrane and immersing the membrane in a buffer solution of pH 4, 7, and 9 totalling 50 mL. This set is then placed on a magnetic stirrer at 200 rpm. At the specified time, 1 mL of the supernatant is taken from outside the membrane and the volume is maintained at 50 mL with the addition of 1 mL of demineralized water. The amount of naproxen released was measured using a UV-vis spectrophotometer by measuring absorbance at 330.5 nm and adjusting to the calibration curve for a standard solution of naproxen.

Characterizations

Morphology of boron–carbon nanodots observed using atomic force microscopy (AFM 5500 M, Japan). The diameter of boron–carbon nanodots was calculated from AFM images using IMAGE J. analysis software. X-ray diffraction (XRD, Rigaku D/Max-2BX, Japan) was used to determine the crystal structure of the nanoparticles with Cu Kα radiation at 5–65°. The sample function group was determined using a Fourier transform infrared spectrometer (FTIR, Shimadzu IR Tracer-100, Japan). UV-vis absorption spectra were measured using a UV-vis spectrophotometer (SHIMADZU 1800, Japan). Morphology of the nanoparticles were observed by transmission electron microscopy (TEM) instrument (Hitachi HT770, Japan). PL spectra were measured using a spectrofluorometer (PerkinElmer LS 55, USA) with a 20 kW Xe lamp. Turbidity value of colloidal nanoparticle were measured by TB1 portable turbidimeter (VELP Scientifica, Italy). The functional groups on the sample surface are determined using X-ray photoelectron spectroscopy (XPS, Shimadzu Axis-Ultra DLD, Japan).

Statistical analysis

All data were obtained in triplicate, with a sample *t*-test on some data.

Results and discussion

The synthesized BCD are blackish-brown solids as represented in Fig. S1 (ESI†). The hydrothermal method fundamentally is based on heating treatment, leads to the carbonization process at high temperatures. This process generates a rearrangement of the carbon structure of the citric acid and doping agent to form a graphene-like structure. Furthermore, a simple step for BCD synthesis was carried out by comparing the visual solution with visible light and under UV light. The fluorescence phenomenon's existence due to material emission originating

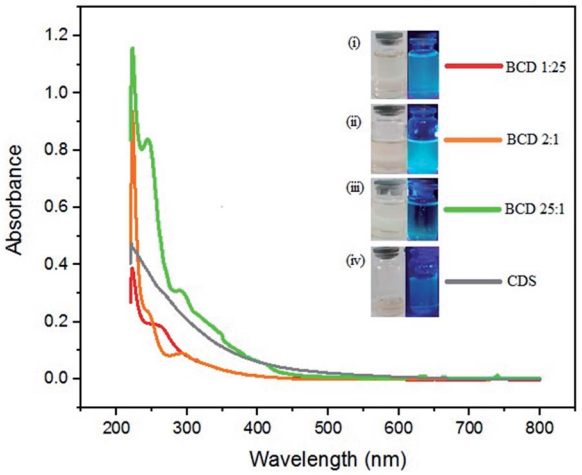

Fig. 1 The UV-vis spectra and its photographs of (i) BCD 1 : 25 (red), (ii) BCD 2 : 1 (orange), (iii) BCD 25 : 1 (green), and (iv) CDS (light purple) under daylight and UV-light by hydrothermal method.

from electron transitions in atomic orbitals indicates the formation of BCD themselves.[20] An in-depth analysis of optical properties, especially on electronic transitions in BCD, will be discussed further in UV-vis. Based on Fig. 1, UV-vis spectra analysis exhibited the absorption at wavelength λ_{max} of 221.25 nm in CDS, whereas in BCD samples 1 : 25, BCD 2 : 1, and BCD 25 : 1 have λ_{max} of 222.80 nm, which correspond to the core electron/C=C transition state ($\pi \rightarrow \pi^*$). Furthermore, the shoulder peaks of CDS, BCD 1 : 25, BCD 2 : 1, and BCD 25 : 1 were showed at 341, 330, 377, and 378 nm, respectively, that recognized as surface state transition (carbonyl group) of the samples ($n \rightarrow \pi^*$).[14,21]

In order to determine the emission value of each BCD, we were using photoluminescence analysis with varied excitation wavelengths at 360, 380, 400, and 420 nm, respectively. The results of the PL analysis note that CDS emitted a strong blue fluorescent at a wavelength of 398.5 nm, BCD 1 : 25, BCD 2 : 1, BCD 25 : 1 occurs at a wavelength of 434 nm (Fig. 2). Furthermore, using R6G as a reference,[22,23] the relative quantum yield (QY) of BCD 1 : 25, BCD 2 : 1, and BCD 25 : 1 were 32.49%, 52.29%, and 4.68%, respectively. The abundant element of boron in CDS causes an electron deficiency state due to the high energy for boron to bind to CDS. Hence, creating a higher red-shifted emission in BCD doping. Therefore, it is necessary to qualify with an ideal variety of components to avoid defects on the CDS surface.[24] Thus, we chose 2 : 1 BCD for further analysis due to the best optical properties and quantum yield compared to other varieties.

FTIR analysis of BCD 2 : 1 and naproxen loaded-BCD was carried out for estimating the surface modification and functional groups that possess the CDS. According to Fig. 3, BCD contained functional groups at 3658, 3023, 1036, 930, 1614, 1020, 1708, 1267, 1230, and 1085 cm^{-1}, that signified to OH, CH benzene, COC, CO methoxy, C=C–C conjugated benzene, CB, CO carbonyl, OBO asymmetric, OBO deformation, and BOH respectively.[25–29] Moreover, naproxen-loaded BCD displayed predominantly the same groups as BCD with the addition at 3126 and 2826 cm^{-1} which identified as CH aliphatic and OCH_3 groups.[25,30]

Further advanced evaluation of surface functional groups of the samples was convinced by an X-ray photoelectron spectrometer (XPS). The collected data was analysed using CasaXPS software. The deconvolution spectra of B 1s, C 1s, and O 1s are available in Fig. 4b and e show BCD and naproxen loaded boron–carbon nanodots (N-BCD), the typical C 1s spectra are similar, showing four distinct peaks located at 283.5; 284.7; 285.8; and 288.2 eV, where these peaks indicate the presence of C–B, C=C/C–C, C–O, and C=O groups, respectively.[15] The O 1s spectrum in BCD (Fig. 4c) showed three peaks, namely at 527.30; 531.20 and 532.5 eV, signifying O=C, O–C, and O–B/C–O–H, while the O 1s spectrum of N-BCD (Fig. 4f) shows three peaks at 529.59; 531.22; and 532.50 eV, representing O=C, O–C, and O–B/C–O–H. The O 1s spectra display the position of 532.50 eV representing the O–B or C–O–H bonds.[31,32] The B 1s spectrum of BCD (Fig. 4a) presents two components at 193.20 and 190.86 eV,

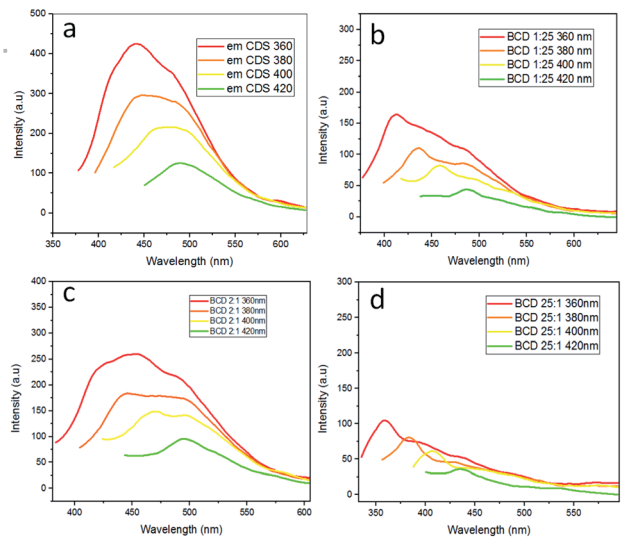

Fig. 2 PL spectra of (a) CDS, (b) BCD 1 : 25, (c) BCD 2 : 1, and (d) BCD 25 : 1 at varied excitation wavelength, including 360 nm (red line); 380 nm (orange line); 400 nm (yellow line); and 420 nm (green line).

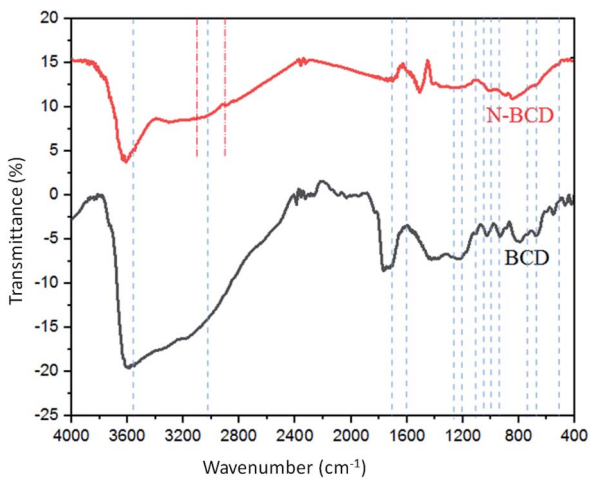

Fig. 3 FTIR spectra of BCD 2 : 1 (black line) and naproxen-loaded BCD (red line).

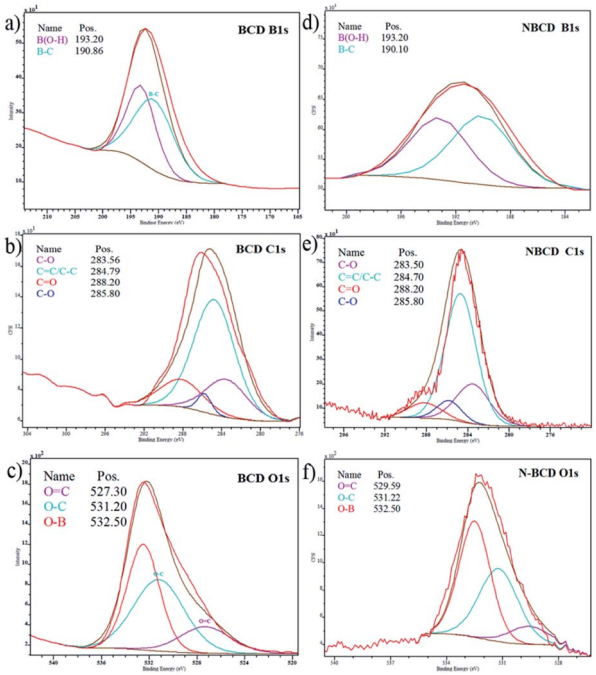

Fig. 4 XPS survey of BCD for (a) B 1s, (b) C 1s, (c) O 1s and incorporation of BCD to the naproxen (N-BCD) for (d) B 1s, (e) C 1s, and (f) O 1s core levels.

associated with B–O and B–C, respectively. In addition, the incorporation of BCD into naproxen was evident by two peaks appearing at the binding energy of 193.20 and 190.10 eV (Fig. 4d), representing B–O and B–C groups.[33] Therefore, the B–OH bond at 193.20 eV indicated that boric acid could replace the original ligand and free boric acid appeared on the CDS surface.[29]

The morphological and crystal structure of BCD was examined by using X-ray diffraction (XRD) and atomic force microscopy (AFM). The diffractogram pattern on the BCD in Fig. 5a indicates a slightly amorphous solid. This phase shows that the synthesis of carbon nanodots using either the hydrothermal method results in dehydration molecules from the surface, transmitting an amorphous or lower carbonate anhydrous material. This amorphous anhydrous material then decomposes. Furthermore, the BCD pattern was then compared with the standard on the JCPDS database 01-0646, which was indicated by typical peaks at 2θ at 27.80° with the Miller index (002) and 40.10° with the Miller index (100). Based on the database, BCD confirmed a graphene-like structure.[34–37] The 2D and 3D morphological structures of BCD showed the spherical size which identified the carbon dots structure (Fig. 5b and c).[14] From the results of AFM characterization, the particle size distribution of BCD was analysed using the computer program ImageJ and Origin shown in Fig. S2 (ESI†). The calculation results show that the average size of BCD in this study is 8.36 nm, which corresponds to the size of the carbon dots, which is below 10 nm.[6,38] Therefore, BCD is promisingly qualified to flow in tissue circulation organs.[32]

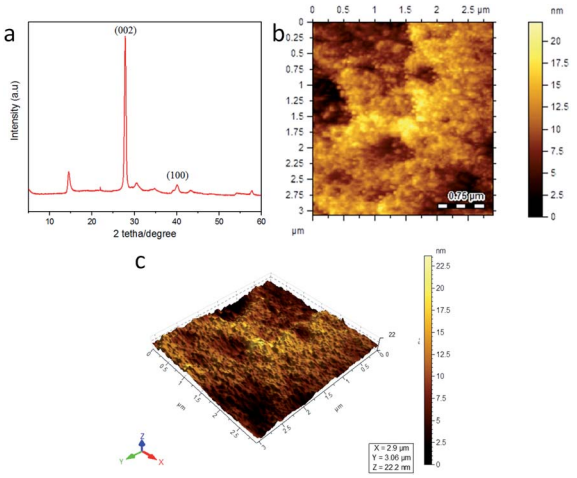

Fig. 5 (a) XRD pattern, (b) 2D, and (c) 3D morphological view of BCD.

CLSM image

Confocal laser scanning microscopy test aims to visualize BCD to cancer cells as a bioimaging agent. From the visual results, BCD provides a great representation of cells. As demonstrated in Scheme 1, BCD could very well permeate cells compare to CDS through a process called endocytosis (Fig. 6). Endocytosis is a mechanism of material originating from outside the cell to enter the cell.[14] The sialic acid receptor on HeLa cells allows BCD to bind specifically to the cell cytoplasm.[39] With its tremendous green fluorescent effect at the excitation wavelength of 488 nm, low toxicity property, and high selectivity to the HeLa cell lines (after 24 h observation), BCD is highly potential to be applied as staining and imaging cancer cells, specifically for HeLa cells.

Preparation of BCD and N-BCD

The design of BCD for naproxen delivery was be done by introducing the drug *via* physical interaction. The benzene

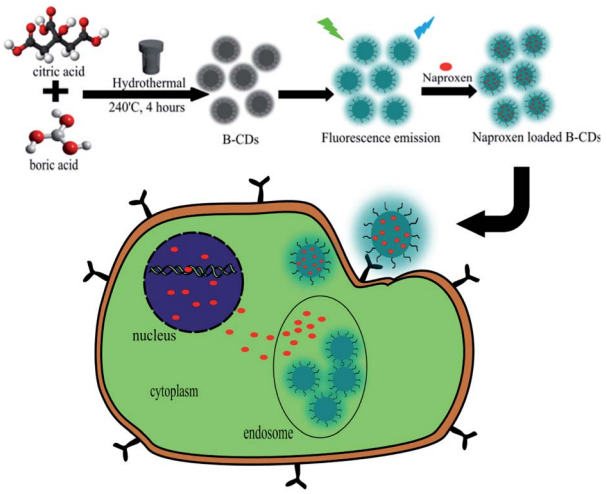

Scheme 1 Synthesis route of BCD and N-BCD for inducing into HeLa cancer cell.

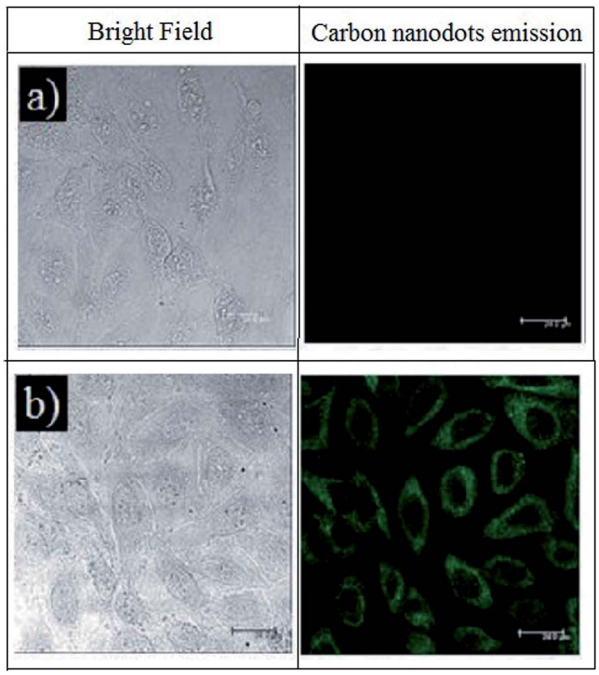

Fig. 6 CLSM image of HeLa cancer cells with (a) CDS and (b) BCD compares to the CDS after 1 h incubation under excitation wavelength at 488 nm. The magnification scale bar showed up to 20 μm.

structure of naproxen may interact with graphene oxide like structure of BCD performed on previous XPS and FTIR data (Fig. 4 and 5) through phi–phi stacking attraction as well as hydrogen bonding of any polar functional group on both materials. The above statement was further by TEM observation on BCD and N-BCD (Fig. S3, ESI†). Through the TEM data, it is also known that both CD are on nanoparticle with spherical form (size below 20 nm). Moreover, the addition of naproxen on N-BCD not change very much on its initial structure. This is support both AFM data on Fig. 5c and S2,† along with confirming conjugation of naproxen not shift the BCD particle structure dramatically. The investigation on colloidal stability of obtained N-CDs against varied pH was further observed by determination its turbidity value (Fig. S4, ESI†). The data inform stability of BCD against varied pH on 72 h. Higher turbidity value tend to closely related on aggregate formation and let precipitation to be happened. On the data, high turbidity value addressed on low pH (7.56 NTU for pH 3 and 6.34 NTU for pH 4), in which allow hydrogen bonding be formed and intense on initiate precipitation of BCD. Moreover, incorporation on naproxen on BCD (N-BCD) not disturb its colloidal stability, which the turbidity level still on similar pattern like BCD. Therefor the turbidity data support above TEM results on confirming both BCD and N-BCD perform high stability and incorporation on naproxen not degrades bare BCD.

In vitro evaluation of BCD and N-BCD

In this analysis, BCD 2 : 1 and N-BCD were carried out to determine whether naproxen had merged with BCD. In this study, the cytotoxic activity was tested *in vitro* against HeLa cells.

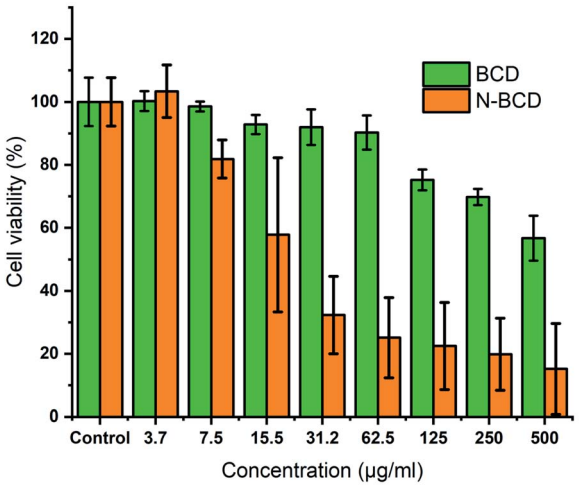

Fig. 7 The MTT assay of HeLa cells viability (2.5×10^4 cells per well) with BCD (green) and N-BCD (orange) at varied concentrations after 24 h incubation (37 °C, 5% CO_2 inner condition). All data are given as mean ± SD with $n = 3$.

These cells are immortal (cannot die of old age) and productive. Hence, they are suitable for this scientific research.[40,41] The cell viability value was determined from the absorbance of the treatment group compared to the control group by using MTT assay. Until the addition of the sample concentration of 500 μg mL^{-1}, if the cell viability is above 80%, it indicates that the sample has low toxicity (Fig. 7).[29,42] Thus, BCD is low toxic and nearly non-toxic based on practical concentrations because at the addition of a concentration of 8111.97 μg mL^{-1}, it can still maintain cell viability (%) above 80% as confirmed by nonlinear curve operation using origin software (Fig. S5, ESI†). The comparative evaluation of naproxen-loaded BCD was also examined to figure out the antitumor efficiency from the loading compound. As the sample concentration increases, cell viability decreases dynamically to a concentration of 500 μg mL^{-1}, where cell viability reaches 20% of the total population.

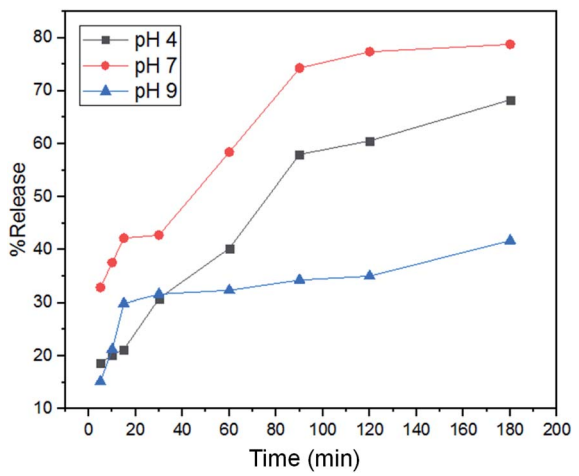

Fig. 8 The dissolution test of naproxen-loaded BCD under pH 4 (black line), 7 (red line), and 9 (blue line) buffer conditions ($t = 3$ h, with ± SD $n = 3$).

Table 1 Naproxen release kinetics of BCD with varied pH

Formula	Parameter	Zero order	First order	Higuchi	Korsmeyer–Peppas
N-BCD pH 4	k	0.0047	0.0084	5.3802	6.7556
	r^2	0.9321	0.9876	0.9806	0.9810
	χ^2	179.6121	60.6533	2.5689	1.3954
	n				0.4501
N-BCD pH 7	k	0.0060	0.0169	7.0602	18.3527
	r^2	0.8812	0.9721	0.9549	0.9597
	χ^2	591.4447	113.1749	33.9511	1.8485
	n				0.2883
N-BCD pH 9	k	0.0031	0.0044	3.6973	9.5836
	r^2	0.6837	0.7263	0.7941	0.8397
	χ^2	378.8021	228.1405	32.2527	5.0484
	n				0.2921

Therefore, the contrast between cytotoxicity of N-BCD and free naproxen to HeLa cells suggests that N-BCD combinations may be more effective antitumor efficiency than free naproxen.[43]

Kinetical release of naproxen-loaded BCD

A dissolution test (release of drug compounds from preparations that dissolve in solvent media) is conducted to analyse the diffusion of drugs against time in an environment that represents body conditions. In this study, determine that the LA and LE of naproxen incorporated on BCD was 28% and 65%, respectively. Through these values we set the naproxen release study.

On the first step, the pH variations were carried out to determine the effect of time on drug dissolution kinetics. The pH variations used in this study were pH 4, which represented acidic conditions, pH 7 expressed neutral conditions, and pH 9 stated alkaline conditions. The obtained data from the dissolution test then matched to the equations of the zero-order, first-order, Higuchi, Korsmeyer–Peppas mathematical model. A drug release mechanism is an important thing to know in drug development.

The dissolution test results illustrate that the kinetic model followed by N-BCD at pH 4, 7, and 9 as a whole follows the Korsmeyer–Peppas kinetic model (Fig. 8). This is based on the magnitude of the r^2 value of the release test at pH 4, 7, and 9 medium is 0.9810; 0.9597; 0.8655, respectively (Table 1). Moreover, the value of chi-square (χ^2) acts as a function of statistical error during the study.[44] The lowest χ^2 value indicates the best-fitted drug release of kinetics model.[45] The lowest value of χ^2 is found in the Korsmeyer–Peppas kinetic model, with the χ^2 value of the release test at pH 4, 7, and 9 medium is 1.3954; 1.8485; and 5.0484, respectively.

As shown in Fig. S6 (ESI†), the comparison of experimental and theoretical test plots demonstrated that the N-BCD completely corresponds to the Korsmeyer–Peppas kinetic model compared to the 0, order 1, and Higuchi models. The Korsmeyer–Peppas model derives the relationship relating to drug release from BCD. The kinetics of the Korsmeyer–Peppas model also depends on the magnitude of the value of n, the value of $n < 0.45$, the drug release is based on the Fickian diffusion mechanism.[46] If $0.45 < n < 0.89$ drug release based on non-Fickian mechanism. The value of $n = 0.89$, the drug release mechanism follows zero-order or can be called case II transport, and $n > 0.89$ drug release is referred to as the super case II transport mechanism.[47] N-BCD had a value of $n < 0.45$, which followed the Fickian diffusion mechanism. Fickian diffusion states that in some direction, the mass of a solute passing through an area per unit time is proportional to the solute concentration gradient in that direction.[48]

The difference in pH of the release medium affects the value of k, which influenced the rate of naproxen release. Medium pH 7 gave the highest k value of 18.3527, followed by pH 9 with 9.5836, and the lowest was pH 4, which was 6.7556. Until the first 10 min at pH 7 has been released 31% and pH 9 is 12.98%, while at pH 4 only 15.96%. In overall observations, the test membrane on the medium pH 7 has a percentage of 78.55%. While at pH 9 it was 41.34%, and pH 4 was only 67.76%. The low dissolution percentage in the medium pH 9 and 4 is possible because pH 9 and 4 affect the diffusion of the medium solution entering the BCD to dissolve naproxen to be pretty slow. This aspect can also explain that naproxen is more dispersed in a neutral medium. As displayed in Fig. 8, naproxen did not release 100% due to intermolecular forces with the carrier, including hydrogen bonds between OH or COOH from CA with COOH from naproxen. These results indicate that naproxen can be released more effectively under neutral conditions (pH 7) than under acidic conditions (pH 4) or in alkaline conditions (pH 9). The greater the dissolution ability of the drug, the higher the bioavailability of the material as a drug delivery carrier.[49]

Conclusions

Boron–carbon nanodots were successfully synthesized from citric acid using the hydrothermal method. Boron–carbon nanodots have structural characteristics similar to an average particle size of 8.35 nm, the quantum yield of 52.29% has a B (OH) group that can bind specifically to cancer cells, and is not toxic. From the results of confocal and toxicity tests, boron–carbon nanodots have proven potential as candidates for bioimaging agents and naproxen delivery systems in HeLa cancer cells.

Abbreviations

CDS Carbon nanodots

BCD	Boron carbon nanodots
N-BCD	Naproxen-loaded boron carbon nanodots
CA	Citric acid
DMEM	Dulbecco's Modified Eagle Medium
NaOH	Sodium hydroxide

Conflicts of interest

There are no conflicts of interest in this present study.

Acknowledgements

The authors thank the Ministry of Research and Technology Republic of Indonesia Research for financially support under contract No. 463/UN3.15/PT/2021 and Universitas Airlangga for providing research facilities for this research.

References

1 Y. Wang and A. Hu, *J. Mater. Chem. C*, 2014, **2**, 6921–6939.
2 W. Liu, C. Li, X. Sun, W. Pan, G. Yu and J. Wang, *Nanotechnology*, 2017, **28**, 485705.
3 Y.-Y. Aung, A. Wibrianto, J. S. Sianturi, D. K. Ulfa, S. C. Sakti, I. Irzaman, B. Yuliarto, J.-y. Chang, Y. Kwee and M. Z. Fahmi, *ACS Omega*, 2021, **6**(28), 17750.
4 D. Dey, T. Bhattacharya, B. Majumdar, S. Mandani, B. Sharma and T. K. Sarma, *Dalton Trans.*, 2013, **42**, 13821–13825.
5 C. Sakaew, P. Sricharoen, N. Limchoowong, P. Nuengmatcha, C. Kukusamude, S. Kongsri and S. Chanthai, *RSC Adv.*, 2020, **10**, 20638–20645.
6 G. Dong, K. Lang, H. Ouyang, W. Zhang, L. Bai, S. Chen, Z. Zhang, Y. Gao, Z. Mu and X. Zhao, *RSC Adv.*, 2020, **10**, 33483–33489.
7 A. Kathiravan, A. Gowri, V. Srinivasan, T. A. Smith, M. Ashokkumar and M. Asha Jhonsi, *Analyst*, 2020, **145**, 4532–4539.
8 Z. Ji, D. M. Arvapalli, W. Zhang, Z. Yin and J. Wei, *J. Mater. Sci.*, 2020, **55**, 6093–6104.
9 Y. Zhou, Y. Liu, Y. Li, Z. He, Q. Xu, Y. Chen, J. Street, H. Guo and M. Nelles, *RSC Adv.*, 2018, **8**, 23657–23662.
10 K. Hola, Y. Zhang, Y. Wang, E. P. Giannelis, R. Zboril and A. L. Rogach, *Nano Today*, 2014, **9**, 590–603.
11 D. K. Dang, C. Sundaram, Y.-L. T. Ngo, J. S. Chung, E. J. Kim and S. H. Hur, *Sens. Actuators, B*, 2018, **255**, 3284–3291.
12 Y. Z. Yang, N. Xiao, S. G. Liu, L. Han, N. B. Li and H. Q. Luo, *Mater. Sci. Eng., C*, 2020, **108**, 110401.
13 G. Tiwari, R. Tiwari, B. Sriwastawa, L. Bhati, S. Pandey, P. Pandey and S. K. Bannerjee, *Int. J. Pharm. Invest.*, 2012, **2**, 2–11.
14 A. Wibrianto, S. Q. Khairunisa, S. C. Sakti, Y. L. Ni'mah, B. Purwanto and M. Z. Fahmi, *RSC Adv.*, 2021, **11**, 1098–1108.
15 Y. Liu, W. Duan, W. Song, J. Liu, C. Ren, J. Wu, D. Liu and H. Chen, *ACS Appl. Mater. Interfaces*, 2017, **9**, 12663–12672.
16 N. Xiao, S. G. Liu, S. Mo, N. Li, Y. J. Ju, Y. Ling, N. B. Li and H. Q. Luo, *Talanta*, 2018, **184**, 184–192.
17 T. Tian, Y. He, Y. Ge and G. Song, *Sens. Actuators, B*, 2017, **240**, 1265–1271.
18 Y. Liu, W. Li, P. Wu, C. Ma, X. Wu, M. Xu, S. Luo, Z. Xu and S. Liu, *Sens. Actuators, B*, 2019, **281**, 34–43.
19 A. Pal, K. Ahmad, D. Dutta and A. Chattopadhyay, *ChemPhysChem*, 2019, **20**, 1018–1027.
20 W. Li, W. Zhou, Z. Zhou, H. Zhang, X. Zhang, J. Zhuang, Y. Liu, B. Lei and C. Hu, *Angew. Chem.*, 2019, **131**, 7356–7361.
21 D. Zuo, N. Liang, J. Xu, D. Chen and H. Zhang, *Cellulose*, 2019, **26**, 4205–4212.
22 M. Fischer and J. Georges, *Chem. Phys. Lett.*, 1996, **260**, 115–118.
23 C. Würth, M. G. González, R. Niessner, U. Panne, C. Haisch and U. R. Genger, *Talanta*, 2012, **90**, 30–37.
24 J. Jana, M. Ganguly, K. R. S. Chandrakumar, G. Mohan Rao and T. Pal, *Langmuir*, 2017, **33**, 573–584.
25 J. Coates, *Interpretation of Infrared Spectra A Practical Approach*, Newtown, USA, 2006.
26 F. Yang, X. He, C. Wang, Y. Cao, Y. Li, L. Yan, M. Liu, M. Lv, Y. Yang and X. Zhao, *Appl. Surf. Sci.*, 2018, **448**, 589–598.
27 J. Romanos, M. Beckner, D. Stalla, A. Tekeei, G. Suppes, S. Jalisatgi, M. Lee, F. Hawthorne, J. D. Robertson and L. Firlej, *Carbon*, 2013, **54**, 208–214.
28 L. Zhao, F. Di, D. Wang, L.-H. Guo, Y. Yang, B. Wan and H. Zhang, *Nanoscale*, 2013, **5**, 2655–2658.
29 M. Z. Fahmi, J.-K. Chen, C.-C. Huang, Y.-C. Ling and J.-Y. Chang, *J. Mater. Chem. B*, 2015, **3**, 5532–5543.
30 D. Halamová, M. Badaničová, V. Zeleňák, T. Gondová and U. Vainio, *Appl. Surf. Sci.*, 2010, **256**, 6489–6494.
31 B. J. Matsoso, K. Ranganathan, B. K. Mutuma, T. Lerotholi, G. Jones and N. J. Coville, *New J. Chem.*, 2017, **41**, 9497–9504.
32 I. V. J. Feiner, K. R. Pulagam, K. B. Uribe, R. Passannante, C. Simó, K. Zamacola, V. Gómez-Vallejo, N. Herrero-Álvarez, U. Cossío and Z. Baz, *J. Mater. Chem. B*, 2021, **9**, 410–420.
33 K. Yang, P. Jia, J. Hou, T. Bu, X. Sun, Y. Liu and L. Wang, *ACS Sustainable Chem. Eng.*, 2020, **8**, 17185–17193.
34 X. Xu, R. Ray, Y. Gu, H. J. Ploehn, L. Gearheart, K. Raker and W. A. Scrivens, *J. Am. Chem. Soc.*, 2004, **126**, 12736–12737.
35 W.-C. Oh, F.-J. Zhang and M.-L. Chen, *J. Ind. Eng. Chem.*, 2010, **16**, 321–326.
36 V. K. Gupta, S. Agarwal and T. A. Saleh, *J. Hazard. Mater.*, 2011, **185**, 17–23.
37 C. Chen, J. Hu, D. Shao, J. Li and X. Wang, *J. Hazard. Mater.*, 2009, **164**, 923–928.
38 D. Kong, F. Yan, Z. Han, J. Xu, X. Guo and L. Chen, *RSC Adv.*, 2016, **6**, 67481–67487.
39 L.-j. Xue, N.-y. Jin, W. Gong, H.-w. Wang and P. Li, *Chin. J. Cancer Res.*, 2003, **15**, 161–166.
40 R. Rahbari, T. Sheahan, V. Modes, P. Collier, C. Macfarlane and R. M. Badge, *BioTechniques*, 2009, **46**, 277–284.
41 A. Capes-Davis, G. Theodosopoulos, I. Atkin, H. G. Drexler, A. Kohara, R. A. F. MacLeod, J. R. Masters, Y. Nakamura, Y. A. Reid and R. R. Reddel, *Int. J. Cancer*, 2010, **127**, 1–8.
42 T.-i. Kim, J.-u. Baek, C. Z. Bai and J.-s. Park, *Biomaterials*, 2007, **28**, 2061–2067.
43 Y. Yuan, B. Guo, L. Hao, N. Liu, Y. Lin, W. Guo, X. Li and B. Gu, *Colloids Surf., B*, 2017, **159**, 349–359.

44 K. Y. Foo and B. H. Hameed, *Chem. Eng. J.*, 2010, **156**, 2–10.
45 G. R. Mahdavinia and H. Etemadi, *Mater. Sci. Eng., C*, 2014, **45**, 250–260.
46 M. Z. Fahmi, N. F. Sholihah, A. Wibrianto, S. C. Sakti, F. Firdaus and J.-y. Chang, *Mater. Chem. Phys.*, 2021, **267**, 124596.
47 K. H. Ramteke, P. A. Dighe, A. R. Kharat and S. V. Patil, *Scholars Acad. J. Pharm.*, 2014, **3**, 388–396.
48 J. Xu, X. Lv, J. Li, Y. Li, L. Shen, H. Zhou and X. Xu, *J. Hazard. Mater.*, 2012, **225**, 36–45.
49 L. Kassaye and G. Genete, *Afr. Health Sci.*, 2013, **13**, 369–375.